Materials and Design 198 (2021) 109333

Contents lists available at ScienceDirect

Materials and Design

journal homepage: www.elsevier.com/locate/matdes

3D printing high interfacial bonding polyether ether ketone components via pyrolysis reactions

Qiushi Li [a,b], Wei Zhao [a,b,*], Bingjie Niu [c], Yiliang Wang [d,e], Xinhui Wu [a], Jiawen Ji [a,b], Yongxiang Li [a,b], Tingting Zhao [a,b], Han Li [a,b], Gong Wang [a,b,*]

[a] CAS Key Laboratory of Space Manufacturing Technology, Technology and Engineering Center for Space Utilization, Chinese Academy of Sciences, Beijing 100094, China
[b] University of Chinese Academy of Science, Beijing 100049, China
[c] University of Toronto Institute for Aerospace Studies, Toronto M3H 5T6, Canada
[d] Department of Chemistry, Tsinghua University, Beijing 100084, China
[e] Institute for Mechanical Process Engineering and Mechanics, Karlsruhe Institute of Technology, Karlsruhe 76131, Germany

HIGHLIGHTS

- A novel strategy to improve the interfacial bonding strength of 3D-printed polyether-ether-ketone components via pyrolysis reaction was developed.
- Almost isotropy mechanical properties in X-Y plane and 59.8 MPa Z-direction bonding strength were reported.
- Higher top layer's temperatures showed a positive influence on interlayer bonding strength.
- The enhancing mechanism of polyhedral-oligomeric-silsequioxane was analyzed from microstructure and pyrolysis analyses.

GRAPHICAL ABSTRACT

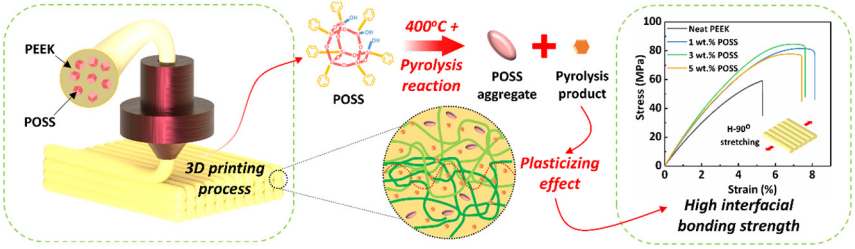

ARTICLE INFO

Article history:
Received 27 July 2020
Received in revised form 11 November 2020
Accepted 13 November 2020
Available online 17 November 2020

Keywords:
3D printing
Bonding strength
Thermal pyrolysis
POSS
PEEK
Mechanical properties

ABSTRACT

Recently, 3D-printed polyether-ether-ketone (PEEK) components have been shown to offer many applications in state-of-the-art electronics, 5G wireless communications, medical implantations, and aerospace components. Nevertheless, a critical barrier that limits the application of 3D printed PEEK components is their weak interfacial bonding strength. Herein, we propose a novel method to improve this unsatisfied situation via the interface plasticizing effect of benzene derivatives obtained from the thermal pyrolysis of trisilanolphenyl polyhedral oligomeric silsequioxane (POSS). Based on this method, the bonding strength of the filaments and interlayers of 3D-printed POSS/PEEK components can reach 82.9 MPa and 59.8 MPa, respectively. Moreover, the enhancing mechanism of the pyrolysis products derived from the POSS is characterized using pyrolysis-gas chromatography/mass spectrometry (Py-GC/MS), Fourier transform infrared spectroscopy (FTIR), and X-ray computed tomography (X-CT). Our proposed strategy broadens the novel design space for developing additional 3D-printed materials with satisfactory interfacial bonding strength.

1. Introduction

Polyether-ether-ketone (PEEK), as one of the most important high-performance 3D-printed polymers, has attracted increased research attention, and has the potential for applications in the domains of energy

* Corresponding authors.
E-mail addresses: zhaowei@csu.ac.cn (W. Zhao), wanggong@csu.ac.cn (G. Wang).

https://doi.org/10.1016/j.matdes.2020.109333

storage, aerospace engineering, and medical implants due to its excellent mechanical properties and chemical stability [1–4]. Additive manufacturing, commonly known as 3D printing, has paved the way for flexibly fabricating versatile components with complex shapes. Among the various 3D-printing technologies, fused deposition modeling (FDM) possesses the ability to rapidly fabricate PEEK components at a relatively low cost [5]. Moreover, with the fast growth of intelligent fusion technology, FDM technology has found its way into soft robotics [6–8], sensors [9,10], and biomimetic devices [11]. However, the inherent weak interfacial bonding problem of PEEK is still a stubborn obstacle for FDM. In particular, the huge temperature difference between the printing temperature (400 °C) and ambient temperature exacerbates this problem. Normally, the interfacial bonding strength of *Z*-direction printed PEEK parts only achieves 20 MPa, which is rather paltry compared with the 100 MPa strength of its bulk, derivative material [12,13]. As such, finding a solution to improve the interfacial properties of printed PEEK components would represent significant progress for FDM technology and the resulting high-performance materials.

Typically, the weak interfacial bonding strength of FDM-derived parts is caused by the huge temperature gradient between the extruder and building chamber during the printing procedure, which leaves only a limited time for the polymer chains to diffuse across adjacent layers. According to previous reports [14–23], the methods used to solve the interface bonding problem can be divided into two approaches. The first consists of physical methods, which rely on external energy to promote the molecular chains' movement. For example, the interlayer bonding performance of 3D-printed polylactic acid (PLA) components coated with carbon nanotubes (CNTs) can be improved by local induced microwave heating [14]. Annealing treatment is also used to encourage diffusion between adjacent layers of printed parts to some extent, such as PLA, polyethylene terephthalate glycol (PETG), and PEEK, but the effect of this method is limited by the undesired porosity of the 3D-printed components [15,16]. Moreover, infrared [17], laser preheating [18,19], ionizing radiation [20], and thermally recycling systems [21] have been integrated into 3D-printing equipment to obtain high bonding strength. The second approach consists of chemical methods, which utilize reactions between additives and printed polymer matrix. Low molecular weight surface-segregating additives (LMW-SuSAs) in filaments could diffuse to the inter-filament layer, and entangle with the linear polymer to improve the poor interlayer adhesion of PLA-printed layers [22]. Then, reactive methacrylate groups can be grafted onto the LMW-SuSAs using in-situ ultraviolet (UV) light to further improve the bonding strength of the PLA during the 3D-printing process [23]. To the best of our knowledge, chemical-modification methods and organic additives that enhance the interfacial bonding of 3D-printed PEEK parts have not been reported, likely due to the bulk of organic additives decomposing at high printing temperature (~400 °C). In addition, the corresponding bonding performance of 3D-printed parts will further reduce with the addition of inorganic enhanced fillers, such as carbon fibers [24,25], CNTs [26], and nano-clay [27], due to the undesired porosity induced by the fillers. Therefore, it is greatly significant to combine the above physical and chemical approaches to improve the interfacial bonding strength of 3D-printed PEEK parts.

Herein, we propose a novel method to fabricate PEEK parts with high interlaminar bonding strength by utilizing the pyrolysis reaction of polyhedral oligomeric silsequioxane (POSS). With the addition of POSS, the 3D-printing behaviors of POSS/PEEK nanocomposites, such as their rheology, morphology, crystallinity, and bonding strength, are greatly influenced by the pyrolysis products. Transmission electron microscopy (TEM) and scanning electron microscopy (SEM) images demonstrate the morphological changes POSS during the 3D-printing process and the transformation of the failure mode of POSS/PEEK printed parts, respectively. From micro-scale to macro-scale, the enhancing effect of POSS on the interfacial bonding strength is determined via typical uniaxial tensile experiments. After that, to obtain better *Z*-direction bonding strength, the top layer's temperature is adjusted to further improve the interlayer bonding performance of the printed parts using optimized-content POSS/PEEK nanocomposites. Finally, the corresponding degradation process and products of POSS are investigated with thermogravimetric analysis (TGA), pyrolysis-gas chromatography/mass spectrometry (Py-GC/MS), and Fourier transform infrared spectroscopy (FTIR). Based on these results, the enhancing mechanism of POSS on the bonding strength of PEEK is further discussed in Section 3.5.

2. Materials and methods

2.1. Raw materials and filaments preparation

PEEK (grade: ZYPEEK 550 G), supplied by Jilin Joinature Polymer Co., Ltd. (Changchun, China), is an unreinforced grade for injection molding and extrusion. Trisilanolphenyl polyhedral oligomeric silsequioxane (grade: POSS SO1458) was purchased from Hybrid Plastics Inc. (Hattiesburg, USA). In this paper, all mentioned POSS refers to trisilanolphenyl polyhedral oligomeric silsequioxane. Prior to preparing the 3D printing filaments, PEEK pellets were chopped into powder by Pulverisette 25 (FRITSCH Co., Ltd., Idar-Oberstein, Germany), and both PEEK and POSS powders were dried for at least 3 h at 150 °C.

The POSS/PEEK nanocomposite filaments were extruded by a Process 11 parallel twin-screw extruder (Thermo Fisher Scientific Co., Ltd., Karlsruhe, Germany) with 11 mm screw diameter, an L/D ratio of 40, and a single screw feeder. The screw speed was set at 100 rpm, and the processing temperature ranged from 340 °C to 390 °C. The contents of POSS/PEEK nanocomposites were prepared with 1, 3, 5 wt%, respectively. The filaments for 3D printing were controlled with a diameter of 1.60 ± 0.05 mm (Shown in Fig. S1).

2.2. 3D printing setup

All the components in this paper were printed by a commercial FUNMAT HT FDM 3D printer (INTAMSYS, Shanghai, China). The geometric models of tensile and flexural test specimens were designed by CATIA V5, according to the ISO 527-2 and ISO 178:2003 as shown in Fig. S2 with the cross-section of 4 × 2 mm^2 and 10 × 4 mm^2, respectively. All samples were printed with identical printing parameters (Table 1). To adjust the cooling time of the top layer, two vertical "doggy-bone" tensile specimens were printed together with a distance from 5 mm to 50 mm. Based on this method, top layer's temperature means that the lowest temperature at top layer before the next layer was applied. All 3D printed components were tested without further thermal treatment.

2.3. Rheological characterization

The rheology of POSS/PEEK filaments was measured by a HAAKE MARS 60 rotational rheometer with a pair of electrical heating plates (Thermo Fisher Scientific Co., Ltd., Karlsruhe, Germany). Wafers with the diameter of 20 mm and height of 2 mm were printed as tested experiments. All specimens were tested with the shearing rate ranging

Table 1
Parameters of FDM processing.

Items	Parameters
Diameter of nozzle	0.4 mm
Nozzle temperature	400 °C
Ambient temperature	90 °C
Heat platform temperature	145 °C
Nozzle moving speed	30 mm/s
Layer thickness	0.1 mm
Raster angle	0°/0°
Air gap	0.18 mm

from 0 to 100 at 400 °C. Besides, zero-shear viscosity of POSS/PEEK samples was measured by shear creeping experiment. A shear force (5 Pa) was applied to samples and maintained 5 mins. After releasing the force, the shear strain versus time was recorded and the zero-shear viscosity was calculated by the equation:

$$d\gamma/dt = \tau_0/\eta_0 \quad (1)$$

where $d\gamma/dt$ indicates the slope at the 5 min of creeping curves, and τ_0, η_0 represent the shear force and zero-shear viscosity, respectively.

2.4. Thermal characterization

Thermogravimetric analysis (TGA) was performed with a Mettler-Toledo TGA/DSC-1 thermogravimetric analyzer (Greifensee, Switzerland) to analyze the thermal stability of POSS and the raw 3D printing filaments. The measurements were carried out at a heating speed of 10 °C/min under nitrogen from 30 °C to 800 °C. To detect volatile pyrolysis products of POSS, the analyzer was coupled to a Fourier-transform infrared spectrometer (TGA-FTIR, Nicolet iS10, Waltham, USA). About 10.0 mg samples were placed in an alumina crucible and heated from 50 to 600 °C at a heating rate of 10 °C/min under nitrogen. The thermogravimetric analyzer and FTIR spectrometer were connected by a quartz capillary at 300 °C. Before testing, the samples were cut from the filaments and dried for 2 h at 100 °C. Pyrolysis-gas chromatography/mass spectrometry (Py-GC/MS) was used to characterize the gaseous pyrolysis products from POSS at 400 °C.

Crystallinity analysis was carried out by a DSC 250 differential scanning calorimeter (DSC, TA Co., Ltd., USA) with a heating rate of 10 °C/min from 50 °C to 400 °C under nitrogen. Glass transition temperature (T_g) was determined by DMA 1 dynamic mechanical analyzer (DMA, Mettler Toledo Co., Ltd., Switzerland) at a heating rate of 5 °C/min from 25 °C to 250 °C with 1 Hz frequency. In order to reproduce the influence of POSS on crystallinity and avoid the disturbance from the printing environment, we chose the secondary heating curves of raw 3D printing filaments to calculate the crystallinity. Crystallinity was determined by equation:

$$\chi(\%) = \frac{\Delta H_{endo} + \Delta H_{exo}}{\Delta H_c}/v_m \times 100\% \quad (2)$$

where ΔH_{endo}, ΔH_{exo} are the integral area of endothermic peak and exothermic peak respectively, v_m is the PEEK matrix content [28], and ΔH_c (130 J/g) is the melting enthalpy of a 100% crystalline PEEK sample [29].

2.5. Mechanical characterization

Mechanical tests were carried out on Instron 5965 universal testing machine (INSTRON Co., Ltd., Norwood, USA) with a 5 kN load capacity. The test speeds were set as 1 mm/min and 2 mm/min for stretching and bending experiments respectively. The Young's modulus was determined between 0.5% and 2% strain. Prior to mechanical testing, the length and width of cross-section were averaged from the three times measuring by a micrometer. The reported values of Young's modulus and ultimate tensile strength (UTS) were averaged from at least five repeated specimens.

2.6. Morphological characterization

Scanning electron microscope (Quanta 650 FEG, USA) was used to observe the fracture surface of the 3D printed specimens. Moreover, the energy dispersive X-ray spectroscopy (EDX, Oxford X-Max, UK) assisted to analyze the dispersion of POSS powder in POSS/PEEK nanocomposites. Transmission electron microscope (FEI Tecnai G2 F30, USA) was used to observe the morphology of POSS powder before and after blending with PEEK.

2.7. Voids distribution characterization

3D-reconstruction imaging of voids was performed on a Skyscan 1172 X-ray μ-CT system (Bruker Corp., USA). The X-ray source was around 10 kW with a voltage of 40 kV and a current of 230 mA. The X-ray detector was 14-bit cooled CCD fiber-optically coupled to scintillator. The scanning resolution was around 1.96 μm/pixel, and the image acquisition region was about 2.5 mm (1278 images) per post-stretching specimen. After image acquisition, the 2D images were further processed to calculate porosity and pores' distribution of specimens by Skyscan CTAn software.

2.8. Thermal imaging of 3D printing process

An E60 infrared thermal imager (FLIR Co., Ltd., USA) was used to monitor temperature of the top layer during 3D printing process. Each thermal image was shot in the mid-printing process to avoid the disturbance of the heating platform.

3. Results and discussion

3.1. 3D-printing POSS/PEEK nanocomposites

In the past, reducing the amount of thermal degradation experienced by polymers as much as possible was highly desired. Here, we do the opposite. As shown in Fig. 1(a), POSS is introduced into the raw 3D-printing PEEK filaments using a melt blending process; meanwhile, benzene derivatives are generated by pyrolysis. The produced POSS/PEEK filaments are rapidly cooled to room temperature by forced air cooling; thus, the pyrolysis products of POSS remain in the filaments. Moreover, owing to the conjugated effect between the phenyl group in the POSS and the PEEK chains, POSS and its pyrolysis products have good compatibility and dispersibility with the PEEK. During the 3D-printing process, higher temperatures and a narrow flow channel further activate the pyrolysis of POSS. Then, the remaining and fresh benzene derivatives are both released. The plasticizing effect of these products promotes mobility of the PEEK chains at the interface, which yields better bonding strength. After extrusion, some of the POSS molecules are squeezed into an ellipsoidal shape by shear and extrusion forces. Moreover, the benzene derivatives that penetrate into the PEEK affect the mobility and crystallization behavior of the PEEK chains.

The enhancing mechanism of POSS on the bonding strength of PEEK is briefly illustrated in Fig. 1(b). Normally, a change in the color of polymer-based composites indicates that the polymer or additive has undergone a pyrolysis reaction. Therefore, the yellow color of the POSS/PEEK-printed gear reveals the thermal decomposition of POSS. In particular, the benzene derivatives from the pyrolysis of POSS can promote the PEEK molecular chains and improve the mobility of the chains across the interface, which act as plasticizers. The thermal decomposition route of the POSS molecules is proposed in Fig. 1(c). At high printing temperatures, the POSS molecules have enough energy to crosslink with each other and release pyrolysis products consisting of water and benzene derivatives, which partly remain and uniformly disperse in the extruded filaments. This scheme is preferred to improve the interfacial bonding strength rather than the conventional external heating method, which means there is no need to modify the 3D printer. The thermal degradation route and enhancing mechanism of the POSS are systemically studied and discussed in Section 3.5.

3.2. Rheology and morphology

The rheological property of materials plays a critical role in 3D printing. In most cases, a suitable shear-thinning effect is regarded as a guarantee for extrusion-based 3D printing [30,31]. Fig. 2(a) demonstrates that the PEEK and POSS/PEEK nanocomposites exhibit good shear-thinning behaviors, as demonstrated by the significant decrease in

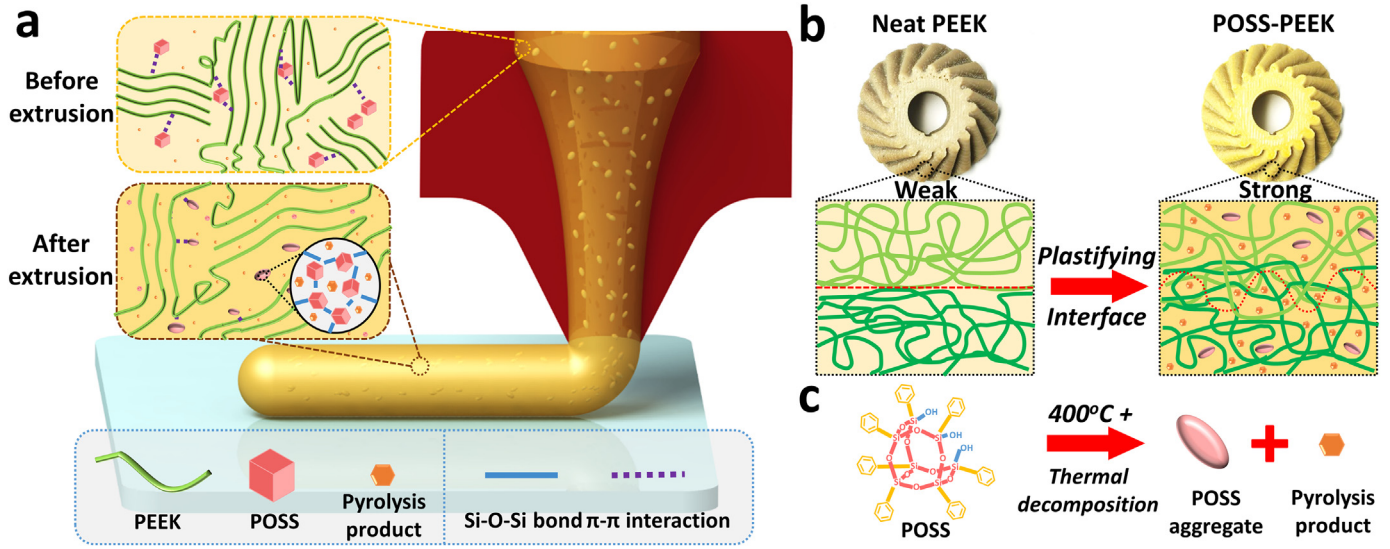

Fig. 1. Illustration of the 3D-printed POSS/PEEK nanocomposites. (a) Morphological changes induced by the POSS during the 3D-printing process. The insets indicate that the pyrolysis products of POSS further improve the mobility of the PEEK chains after high-temperature processing. (b) The pyrolysis products of POSS serve as plasticizers to increase the interface bonding strength. Firstly, the benzene derivatives promote the PEEK chains to achieve better diffusion between layers. Then, POSS aggregates induce crack deflection to dissipate the fracture energy. (c) Pyrolysis process and products of POSS.

their apparent viscosity as a function of the shear rate (which ranges from 10^{-3} to 10^{2} s^{-1}). Moreover, the POSS/PEEK nanocomposites possess a more remarkable shear-thinning behavior than the neat PEEK due to the almost fivefold zero-shear viscosity of the former at low shear rates; meanwhile, the same degree of apparent viscosity is shown at high shear rates. This phenomenon indicates that the POSS/PEEK melt is a non-Newtonian fluid and can be extruded smoothly through the nozzles. Besides, the creep resistance of the POSS/PEEK melt gradually improves as the amount of POSS increases (Fig. S3), which demonstrates that the POSS/PEEK nanocomposites have an excellent capability for shape retention. Therefore, they possess better adaptability to maintaining the dimensions of the printed parts, which is beneficial for fabricating complex and detailed models.

After the printing process, the morphology and dispersion of POSS play essential roles in the mechanical properties of 3D-printed PEEK parts. TEM and SEM images show the distribution and morphological

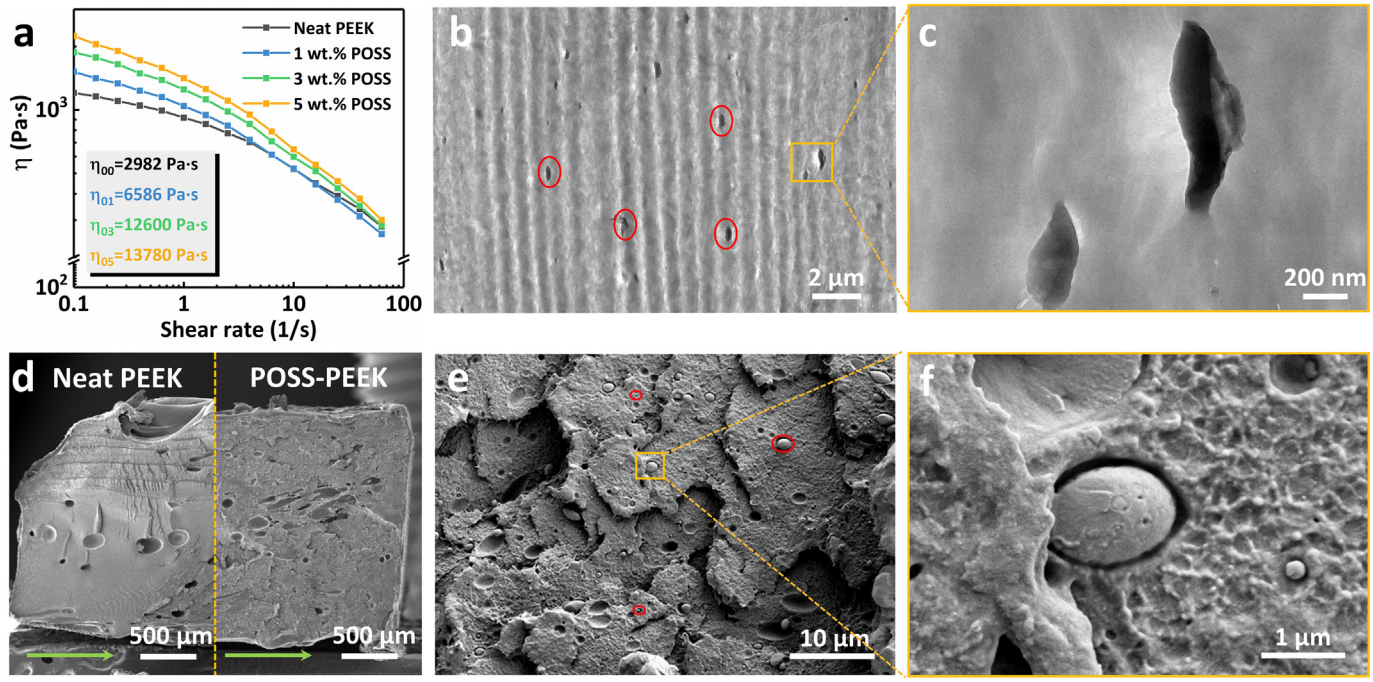

Fig. 2. Rheological properties and micro-morphology of the POSS/PEEK nanocomposites. (a) Dynamic viscosity of samples of different POSS content as a function of the shear rate. The inset shows the corresponding zero-shear viscosity of each sample. (b) TEM image of a POSS/PEEK raw filament. The red circles mark the local distribution of POSS in the PEEK matrix. (c) The enlarged figure in (b) shows the morphology of the POSS in detail. (d) SEM image of the fractured section, which shows a rough surface in the POSS/PEEK-printed parts. In contrast, the smooth surface of the PEEK indicates a brittle fracture mode. The green arrows mark the direction of the printing tracks. (e) Fractured surface of the POSS/PEEK-printed part. (f) The POSS aggregate after extrusion reveals that the POSS has undergone further pyrolysis compared with the sample shown in (c).

changes of the POSS in the filaments and the 3D-printed parts, respectively. As shown in Fig. 2(b) and (c), "spindle-like" POSS aggregates with various sizes (from 100 nm to 2 μm) show a relatively uniform distribution in the PEEK matrix. These aggregates formed by crosslink and pyrolysis reactions with the POSS. Except for the visible POSS aggregates, the energy-dispersive X-ray (EDX) spectroscopic images show that most of the POSS molecules are well distributed in the filaments (Fig. S4). This phenomenon agrees with the finding of a previous report [32].

The subsequent printing process accelerates the pyrolysis reaction of the residual POSS molecules. Higher temperatures and shear effect in the hot nozzle change the distribution of the POSS in the PEEK, and promote the pyrolysis of the former. Fig. 2(d) gives a comparison between the fractured surfaces of Z-direction printed parts made of PEEK and POSS/PEEK. The latter presents a more regular profile, which is consistent with the creep recovery results (Fig. S3). Moreover, the PEEK part shows a smooth fractured section, while the POSS/PEEK part has more raised areas and a rugged surface (Fig. 2(e) and Fig. S5), which demonstrates that the fracture modes have been changed by the addition of the POSS. It is noted that there are ellipsoid-shaped POSS aggregates with a size of ~2 μm (Fig. 2(f)) in the fractured section of the 3D-printed POSS/PEEK parts (Fig. S6(a)). These aggregates dissipate the fracture energy by deflecting cracks, and reducing the formation of larger voids. The enhanced shear-thinning effect of POSS/PEEK and the morphological transformation of the POSS molecules provide a firm foundation for obtaining better interfacial bonding and mechanical properties of 3D-printed components.

3.3. Mechanical performance of the POSS/PEEK-printed components

For practical applications, it is important to investigate the mechanical properties of 3D-printed POSS/PEEK components in all directions. To verify the enhanced 3D-printing behavior resulting from the POSS, the mechanical properties of the 3D-printed samples made from

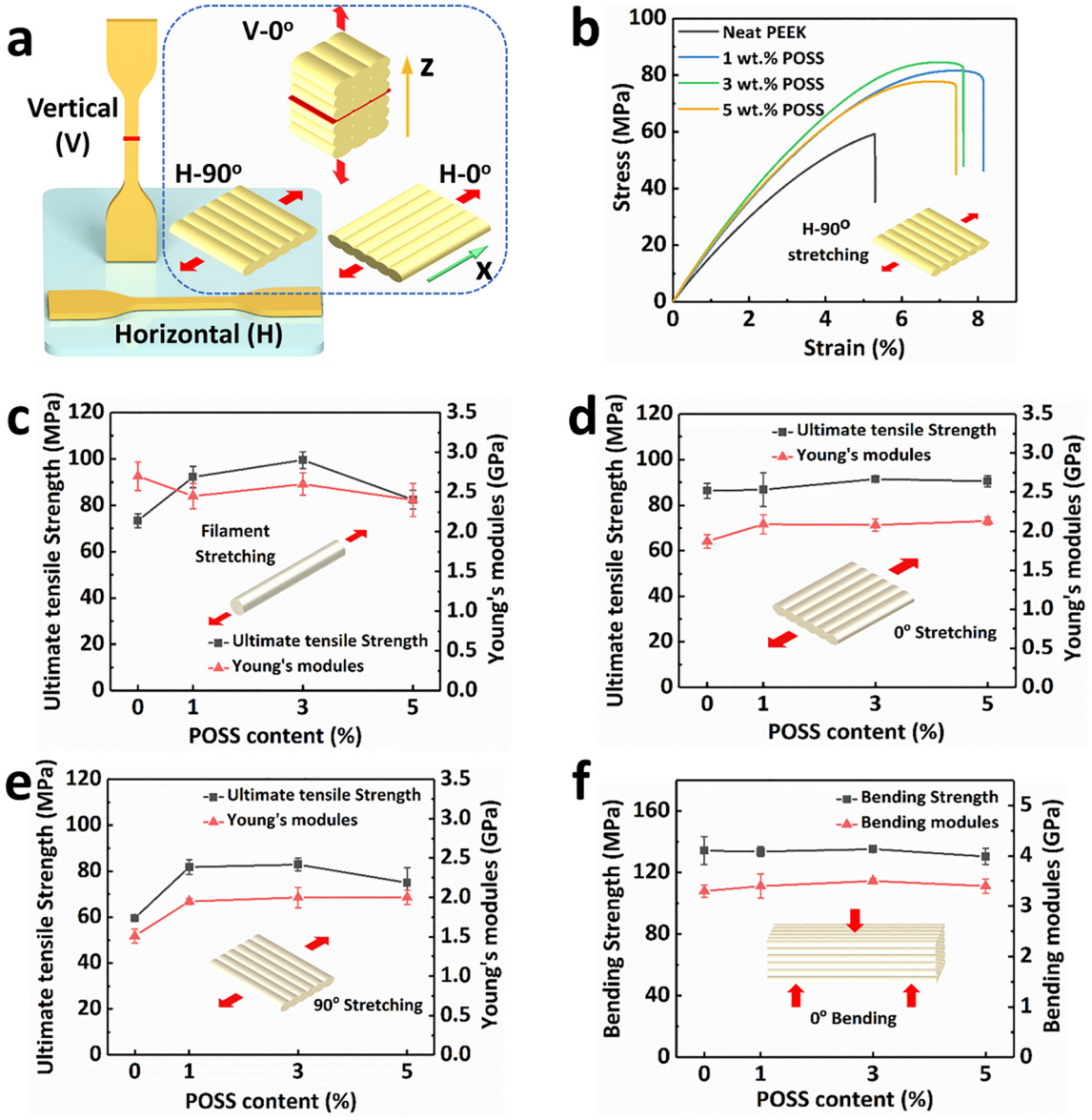

Fig. 3. Mechanical properties of 3D-printed POSS/PEEK components with various POSS contents. (a) The tensile specimens, built with different orientations, show the typical isotropic properties of the 3D-printed parts. V-0° represents vertically printed tensile specimens, while H-0° and H-90° represent samples horizontally printed along and perpendicular to the tensile direction, respectively. (b) The typical stress-strain curve of the H-90° specimens indicates that the increasing bonding properties change the failure mode to a ductile fracture mode. (c-f) The UTS and Young's moduli of the 3D-printed filaments, H-0°, H-90°, and bending specimens as a function of the POSS content, respectively.

POSS/PEEK and neat PEEK were evaluated. The results of the mechanical experiments of three tensile specimens (H-0°, H-90°, and V-0°), are shown in Fig. 3(a), where we tested the in-plane strength, filament bonding strength, and layer bonding strength of the 3D-printed components. Previous studies revealed that the bonding strength of in-plane printed filaments represents the diffusing capability of printed material between filaments [22,23]. Typical stress-strain curves of various-content POSS/PEEK-printed H-90° parts are depicted in Fig. 3(b). The addition of POSS with any content effectively improves the bonding strength between filaments, where a maximum bonding strength of 82.9 MPa is obtained with the 3 wt% POSS. Moreover, the stress-strain curves also reveal that the fracture mode of POSS/PEEK changes from brittle failure to ductile fracture, which agrees with the analyses of the SEM images.

To understand the fundamental influence trend of the POSS on the mechanical properties of the printed POSS/PEEK parts, we tested the tensile strength of individual filaments extruded at a constant rate. As shown in Fig. 3(c), with the addition of POSS, the ultimate tensile strength (UTS) of the POSS/PEEK parts increases, where a maximum value of 99.5 MPa is achieved by the 3 wt% POSS. However, an increase of POSS to 5 wt% leads to a reduction of the tensile strength. To explain the phenomenon, SEM images of the 3 wt% and 5 wt% POSS/PEEK printed parts are shown in Fig. S6. The images demonstrate that, with the appropriate content of POSS, ellipsoid-like solid structures form in the printed parts. These structures are good at dispersing stress, absorbing energy, and guiding crack deflection. However, these ellipsoid-like structures will form slender aggregates if too many POSS molecules are added to the PEEK, which reduces the area of thrust surface for stress delivery and leads to stress concentration [32].

The tensile properties of the H-0° printed specimens (Fig. 3(d)) present a similar increasing tendency as the individual filaments, but the enhanced strength is less than for the single filaments, which could contribute to the formation of voids during printing process. Voids and interfaces induced by the printing process prevent the PEEK chains from the fully stretching, thereby reducing the reinforcing effect of the POSS. The UTSs of H-90° printed specimens increase obviously with increasing POSS content, and reach a peak of 82.9 MPa with the addition of 3 wt% POSS (Fig. 3(e)), which is 40% larger than that obtained with the neat PEEK H-90° printed specimens. Moreover, the UTS of H-90° can reach 90% that of the H-0° printed parts with the same POSS content, which shows an almost isotropic mechanical performance. This property is highly required for various materials fabricated by the FDM process, especially with PEEK.

The results of the bending test of H-90° printed parts (Fig. 3(f)) are similar to their corresponding tensile test results. These results (Figs. 3(d-f)) show that the effect of the POSS in terms of enhancing the strength of the H-90° printed parts is more obvious than for the H-0° printed parts. The interfaces of PEEK-printed parts show that their original weak bonding strength is due to poor diffusion. As such, the enhancing effect of the POSS for promoting diffusion can be easily highlighted. All the specific values of the mechanical properties are listed in Table S1. Overall, a 3 wt% content of POSS in PEEK yield the best mechanical properties and bonding strength between the filaments. Therefore, the next Section will focus on obtaining better interfacial bonding strength of *Z*-direction (V-0°) printed parts based on the 3 wt% POSS.

3.4. Interfacial bonding strength optimization

In this section, we focus on the interlayer bonding performance of 3D-printed PEEK parts. During the printing process, the temperature of deposited beads is affected by the continuously heated building platform and printing speed, where only the latter has an influence on the temperature of the deposited beads along the vertical axis. The top layer's temperature is influenced by the standing time of each layer, which also greatly influences the bonding strength of 3D-printed V-0° specimens, especially for those made of PEEK [21].

To achieve the goal of high bonding strength, controlling the temperature of the top layer is necessary. Hence, we designed a printing model, as shown in Fig. 4(b). With the help of the model, we can control the top layer's temperature by adjusting the distance between two "doggy-bones", denoted here as *d*. The temperature of the top layer as a function of *d* was recorded by thermal imagery (Fig. 4(a)). It was ensured that the distance was sufficiently long to allow enough cooling time for each sample's top layer. For short values of *d*, disordered layers formed due to the short cooling time, as shown in Fig. S7(a) for $d = 0$. The interfacial bonding strength of POSS/PEEK and neat PEEK as a function of *d* is illustrated in Fig. 4(c). It is noted that the interlayer bonding strength of both the POSS/PEEK- and neat PEEK-printed parts shows a slightly decreasing trend as *d* increases. Combining the temperature curves and strength values, we can determine that the average interlayer bonding strength of the POSS/PEEK parts is higher than of the neat PEEK for the range of temperature investigated here. The maximum bonding strength of the POSS/PEEK samples reaches around 59.8 MPa, which poses a 20% improvement compared to the neat PEEK-printed samples under the same condition.

Surface roughness is also a critical property for 3D printing. Without a sufficient cooling time, the shape of incompletely solidified PEEK can be easily disturbed by repetitive movements of the nozzle, resulting in a poor surface in most cases. As shown in Fig. S7(a) and (b), the surface roughness of the neat PEEK V-0° printed parts is poor for $d \leq 20$ mm. In contrast, the threshold value of shape retention is improved for the POSS/PEEK V-0° printed parts, where the surface is relatively smooth when $d \geq 5$ mm and the top layer's temperature is lower than 240 °C, which possibly contribute to the greater shear thinning effect seen in Fig. 2(a). Moreover, a higher temperature of the top layer also further promotes the PEEK chains' diffusing across the interface of adjacent filaments. Most importantly, this strategy is not only suitable for PEEK, but also applicable for most kinds of thermal plastic material used for extrusion-based 3D printing.

To date, more researchers are utilizing X-ray computed tomography (X-CT) for detecting and characterizing the compactness of 3D-printed samples [33]. Using this technique, we calculated the void size distribution of the stretched PEEK and POSS/PEEK V-0° printed parts (Fig. 4(d)). In terms of the number of voids, it is obvious that fewer voids are generated between filaments and layers in the POSS/PEEK-printed parts. This phenomenon directly confirms that the pyrolysis of POSS effectively improves adhesion between adjacent layers. For the neat PEEK parts, the void sizes range from 20 μm to 120 μm, while most are around 20 μm for the POSS/PEEK parts, and very few of them are larger than 60 μm. Large voids may form during the tensile process, which reduces the total area to bear an applied force, and the subsequent weak resistance to crack propagation will lead to the rapid fracturing of PEEK parts. In the POSS/PEEK parts, the POSS aggregates disperse in the PEEK matrix, which inhibits the voids from enlarging due to tensile stress. Thus, a higher *Z*-direction tensile strength of POSS/PEEK-printed parts is obtained. In summary, by adjusting the content of POSS and the distance (i.e. the top layer's temperature), the *Z*-direction bonding strength can be successfully improved to 59.8 MPa.

3.5. Pyrolysis and enhancing mechanism

To clarify understand the influence of the POSS on the 3D-printing process, analyzing the morphological changes and pyrolysis behavior of POSS during 3D printing is necessary. TGA-FTIR, as a common method for pyrolysis analyses, was used here to analyze the pyrolysis volatile products of POSS. As shown in Fig. 5(a), the major pyrolysis species of POSS are illustrated in the 3D FTIR spectra. Obviously, water (around 3500 cm^{-1}), CO_2 (2500 cm^{-1}), and aromatic compounds (1500–1800 cm^{-1}) are generated in the range 200 °C to 600 °C (Fig. 5(b)). The pyrolysis route of the POSS follows three reactions. Firstly, it is speculated

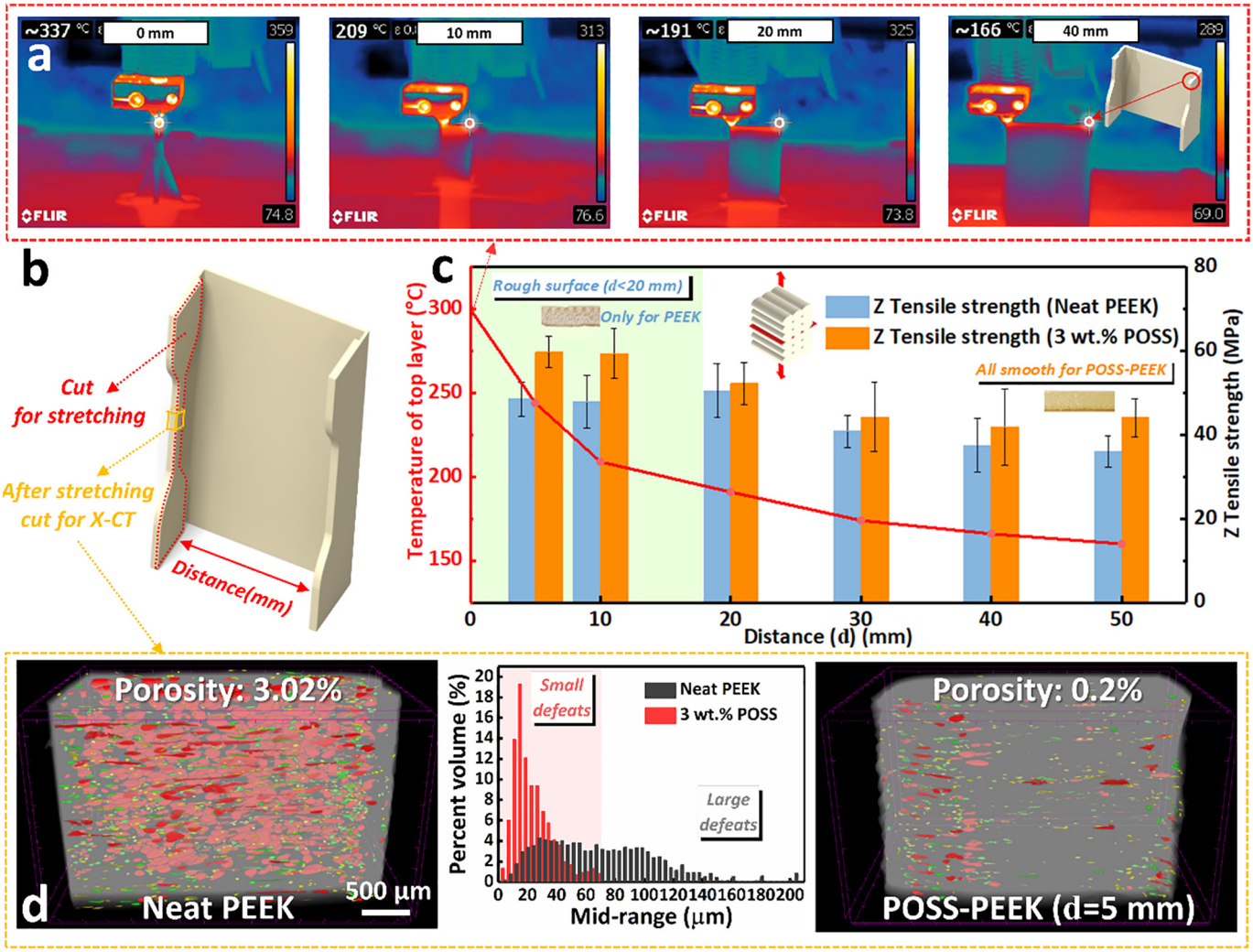

Fig. 4. *Z*-direction tensile experiments of the POSS/PEEK nanocomposites. (a) Infrared thermal images monitor the top layer's temperature during the printing process. The value at the left corner of each sub-figure shows the temperature of the white central circle. (b) The fabrication mode of the *Z*-direction tensile specimens. The distance between two "doggy-bones" is called *d* for short. (c) Interlayer bonding strength and the top layer's temperature of the 3D-printed *Z*-direction specimens as a function of *d*. (d) Voids' size distribution and the 3D rebuilt images of post stretching V-0° specimens via X-CT analyses.

that the POSS molecules may crosslink with each other and release water at 200 °C (Fig. 5(b) and (c)). Secondly, phenyl groups break away from the POSS cage, and partly degrade into the benzene derivatives by rearrangement. Lastly, the benzene derivatives further decompose into CO_2. Additionally, the lower decomposition temperature of the POSS/PEEK indicates that an increased content of POSS slightly decreases the thermal stability of PEEK.

FTIR spectra of the residual POSS at different temperatures (Fig. 5(d)) further explain the pyrolysis process. The results show that the peaks of Si-OH (3240 cm^{-1}) and Si—C (phenyl) (884 cm^{-1}) almost disappear above 300 °C, which indicate that the phenyl and hydroxy groups on the POSS molecule have decomposed at this temperature. Meanwhile, the characteristic peaks of aromatic compounds (3067, 1593, and 1430 cm^{-1}) also obviously decrease, indicating that the phenyl groups decompose into benzene derivatives by rearrangement. This pyrolysis process is consistent with the results of previous reports [34,35]. In summary, the pyrolysis products of POSS are determined as water, CO_2, and benzene derivatives.

Detailed information of the benzene derivatives was determined via a Py-GC/MS experiment at 400 °C. As shown in Fig. 5(e), the main pyrolysis products include cyclohexane, benzene, methylbenzene, and other organic gases, which agree with the FTIR results. The plasticization effect of these organic molecules, especially the aromatic and aliphatic solvents, has an evident influence on the mobility of the PEEK chains and mechanical properties of fabricated parts [36,37]. These organic products uniformly distribute around the interface, and serve as a plasticizer to reduce the intermolecular forces causing a partial relaxation of the polymer chains. This phenomenon makes it easier for the chains of PEEK to cross the interface, and hence better entangle with other chains.

From the thermal analysis, the plasticizing effect of the POSS was further verified by differential scanning calorimetry (DSC) and dynamic mechanical analysis (DMA) experiments. Under high temperature, hybrid POSS molecules decompose into two parts: an inorganic ceramic-like phase and organic small molecules. The former inhibits the PEEK from stacking into a crystal phase, while the latter permeates into the PEEK chains to reduce the intermolecular forces. Both decline the PEEK's crystallinity. However, if only the inorganic phase, as an additive, dopes into the PEEK matrix, the decline of crystallinity is relatively limited under non-isothermal crystallization. Also, it does not influence the glass transition temperature (T_g) of the PEEK [38,39]. As shown in Fig. 5(f), only 3 wt% POSS causes a 10% decline of crystallinity, which possibly contributes to the combined action of the POSS aggregates

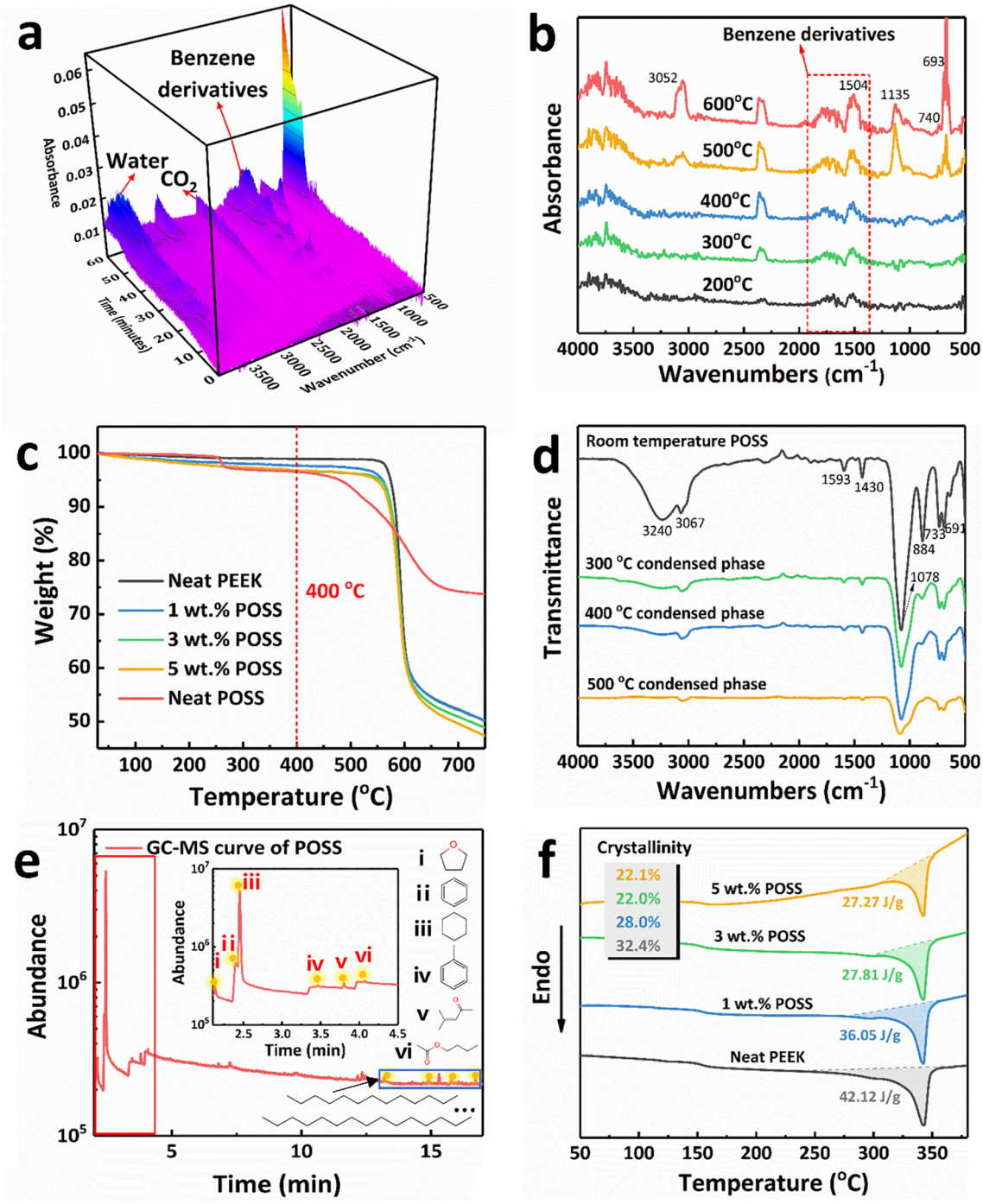

Fig. 5. Pyrolysis process of POSS and its influence on POSS/PEEK nanocomposites. (a) 3D TGA-FTIR spectra of the pyrolysis gases produced by the POSS powder. (b) The extracted FTIR spectra of (a) from 200 °C to 600 °C. (c) TGA curves of the 3D-printing filaments with various POSS contents. (d) FTIR spectra of the condensed phase of POSS at different temperatures. (e) Py-GC/MS chromatogram of the gaseous pyrolysis products from POSS, and major compounds are identified of peaks from I to VI in the Py-GC/MS chromatogram. (f) DSC curves of PEEK with various POSS content. The inset shows the degree of crystallinity calculated by melting enthalpy.

and pyrolysis organic molecules seen in the DSC curves. Moreover, the plasticizing effect on semi-crystalline polymers commonly manifests as a reduction of T_g and the melt temperature (T_m).

To characterize T_g of the POSS/PEEK composite, we performed DMA experiments to analyze the influence of the small molecules, as shown in Fig. S9. The peak of loss factor shifts from 169.8 °C to 164.9 °C with the inclusion of POSS. This phenomenon reveals that the plasticizing effect of the small molecules on the PEEK chains. Fig. 6 demonstrates this enhanced interfacial bond formation process, where stiff aggregates of POSS are unable to diffuse easily through the interface due to high shear forces. Only organic molecules can diffuse relatively easily through the interface; a similar conclusion was determined by Levenhagen and co-workers [22,23]. At the beginning, the newly deposited melt serves as a heat source to re-heat the matrix and form a surface contact. Then, partial pyrolysis products plasticize the PEEK chains around the interface to extend the diffusion process. Lastly, a stronger bond is formed by sufficient diffusion, and the partial acting pyrolysis products remain in the final product. Based on this process, satisfactory

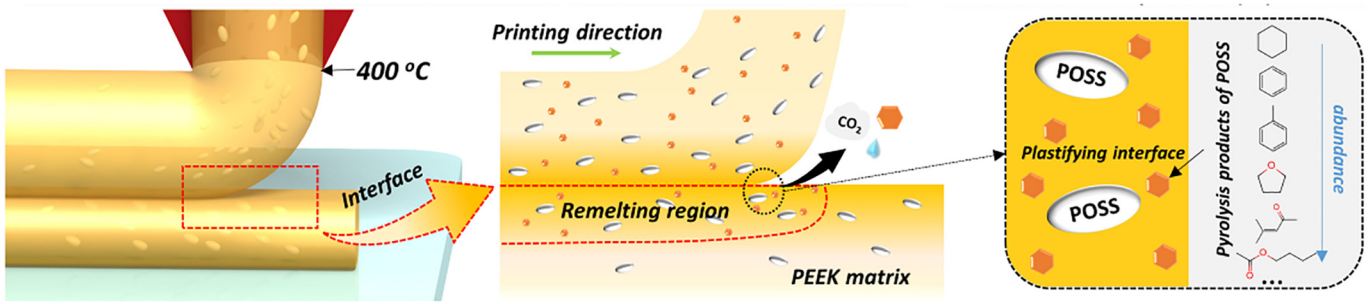

Fig. 6. Illustration of the bond formation process around the interface. Firstly, two beads come into contact with each other as melt extrudes from the nozzle at 400 °C. Then, the newly deposited material re-heats the matrix. During this process, the fresh and residual pyrolysis products serve as plasticizers to promote chains of PEEK diffusing through the interface to form a stronger bond.

bonding performance of printed samples can be obtained by utilizing the pyrolysis reaction of POSS.

3.6. Technology comparison

Until now, we have demonstrated that the pyrolysis of POSS could improve 3D-printing quality and interlayer bonding performance. To further demonstrate this, we drew Ashby diagrams, as shown in Fig. 7 (a) and (b), to compare the bonding strength of the POSS/PEEK parts with commercial 3D-printed polymers. For the POSS/PEEK material, the bonding strength of the H-90° and V-0° printed parts both achieve the highest value among the majority of polymers, representing increases of 14% and 305% compared to previous reports [12,13,15,40–49], respectively. Then, we designed and printed a *Z*-directional component with the shape of a climbing hook (Fig. 7(c)), using 3 wt% POSS/PEEK for bearing a 70-kg person. Supplementary Video 1 shows that the printed component could bear the dynamic loading process, which is a severe challenge for printed components. From Fig. 7(d), it can be seen that the POSS/PEEK component improves the bonding performance to bear 1100-N tension, which exceeds what the neat PEEK part could withstand by about 400 N. In addition, the statics simulation of the climbing hook (Fig. S10) indicates that the two arms of the printed component can endure 55– 60 MPa of stress, and the dangerous points may even exceed 60 MPa when the bottom of hook surface endures a 1000-N external force. Combined with the results shown in Fig. 7(d), it is found that the other printed POSS/PEEK parts could also reach a bonding strength of around 60 MPa, as shown by the test specimens.

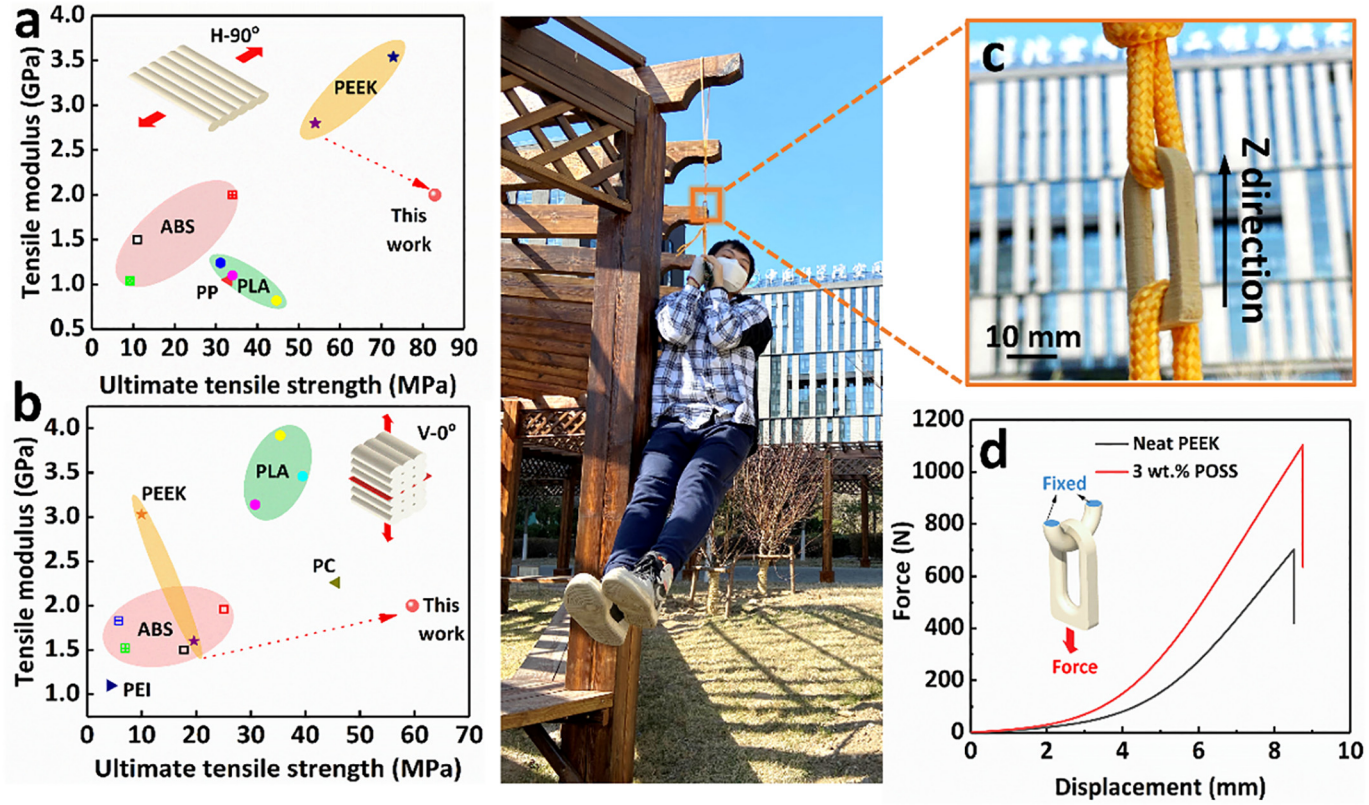

Fig. 7. Demonstration of the excellent interfacial bonding strength of POSS/PEEK printed parts. Ashby diagrams of POSS/PEEK nanocomposites and other commercial 3D-printed polymers showing the (a) the bonding strength of filaments [13,40–44] and (b) bonding strength of layers [12,13,15,40,45–49]. (c) A Z-direction printed PEEK climbing hook, which shows a great capability to bear continuous pull-ups from a 70-kg person, as shown in Supplementary Video 1. (Inspiration comes from the report of [14]) (d) A mechanical comparison of the neat PEEK and 3 wt% POSS/PEEK printed climbing hook.

4. Conclusions

In this work, we reported a simple strategy for improving the 3D-printing quality and interfacial bonding performance of PEEK material by means of utilizing the pyrolysis of POSS. POSS/PEEK 3D-printing filaments with 1 wt% to 5 wt% POSS contents were fabricated. Based on these, the morphological transformation and pyrolysis behavior of the POSS molecules were systemically investigated in terms of their microstructure. Uniaxial tensile experiments were conducted on the POSS/PEEK printed specimens, which were built to test two orthogonal orientations. The results of these experiments demonstrated that 3 wt% POSS/PEEK had the best mechanical performance. Moreover, the interfacial bonding strength of the *Z*-directional printed samples could reach a high value of 59.8 MPa by adjusting the top layer's temperature. Then, FTIR and Py-GC/MS measurements of the POSS demonstrated that its effective pyrolysis products are benzene derivatives, which collectively promoted the mobility of PEEK chains at the interfacial layers. The plasticizing effect was further verified by DSC and DMA experiments. In summary, we determined that the pyrolysis behavior of POSS could be useful for enhancing the interfacial bonding strength of 3D-printed parts, and is a novel route for improving the 3D-printing quality. With the approach proposed in this work, 3D-printed PEEK components with strong interlayer bonding strength can be fabricated without modifying the existing equipment. We believe that thermal decomposition will pioneer a new path for 3D-printing high interfacial bonding parts and broaden the design space of extrusion-based printing methods.

Supplementary data to this article can be found online at https://doi.org/10.1016/j.matdes.2020.109333.

Author contribution statement

W.Z. and G.W. initiated the key concepts of the research. Q.L. and W.Z. prepared the manuscript and illustrated figures. Q.L., B.N. and X.W. designed and carried out the corresponding experiments. Y.W. gave the theoretical direction of pyrolysis. J.J., Y.L., T.Z. and H.L. discussed and fixed the text together.

Declaration of Competing Interest

The authors declare that they have no known competing financial interests or personal relationships that could have appeared to influence the work reported in this paper.

Acknowledgements

This work was financially supported by the Youth Innovation Promotion Association of Chinese Academy of Science (2020169), the Key Research Program of Frontier Sciences, CAS, Grant No. ZDBS-LY-JSC042 and No. QYZDB-SSW-JSC050-01, and the Strategic Priority Research Program, CAS, Grant No. XDA22010101.

References

[1] J. Min, K.Y. Choi, E.C. Dreaden, R.F. Padera, R.D. Braatz, M. Spector, P.T. Hammond, Designer dual therapy nanolayered implant coatings eradicate biofilms and accelerate bone tissue repair, ACS Nano 10 (2016) 4441–4450.
[2] Y.-T. Weng, H.-W. Liu, A. Pei, F. Shi, H. Wang, C.-Y. Lin, S.-S. Huang, L.-Y. Su, J.-P. Hsu, C.-C. Fang, Y. Cui, N.-L. Wu, An ultrathin ionomer interphase for high efficiency lithium anode in carbonate based electrolyte, Nat. Commun. 10 (2019) 5824.
[3] J. Li, X. Niu, J. Song, Y. Li, X. Li, W. Hao, J. Fang, T. He, Harvesting vapor by hygroscopic acid to create pore: morphology, crystallinity and performance of poly (ether ether ketone) lithium ion battery separator, J. Membr. Sci. 577 (2019) 1–11.
[4] C. Barile, C. Casavola, F. De Cillis, Mechanical comparison of new composite materials for aerospace applications, Compos. Part B-Eng. 162 (2019) 122–128.
[5] S. Gantenbein, K. Masania, W. Woigk, J.P.W. Sesseg, T.A. Tervoort, A.R. Studart, Three-dimensional printing of hierarchical liquid-crystal-polymer structures, Nature 561 (2018) 226–230.
[6] T.J. Wallin, J. Pikul, R.F. Shepherd, 3D printing of soft robotic systems, Nat. Rev. Mater. 3 (2018) 84–100.
[7] S.I. Rich, R.J. Wood, C. Majidi, Untethered soft robotics, Nat. Electron. 1 (2018) 102–112.
[8] R.L. Truby, J.A. Lewis, Printing soft matter in three dimensions, Nature 540 (2016) 371–378.
[9] M. Nadgorny, A. Ameli, Functional polymers and nanocomposites for 3D printing of smart structures and devices, ACS Appl. Mater. Interfaces 10 (2018) 17489–17507.
[10] W. Yang, W. Zhao, Q. Li, H. Li, Y. Wang, Y. Li, G. Wang, Fabrication of smart components by 3D printing and laser-scribing technologies, ACS Appl. Mater. Interfaces 12 (2020) 3928–3935.
[11] X. Kuang, D.J. Roach, J. Wu, C.M. Hamel, Z. Ding, T. Wang, M.L. Dunn, H.J. Qi, Advances in 4D printing: materials and applications, Adv. Funct. Mater. 29 (2019) 1805290.
[12] M. Rinaldi, T. Ghidini, F. Cecchini, A. Brandao, F. Nanni, Additive layer manufacturing of poly (ether ether ketone) via FDM, Compos. Part B Eng. 145 (2018) 162–172.
[13] M.F. Arif, S. Kumar, K.M. Varadarajan, W.J. Cantwell, Performance of biocompatible PEEK processed by fused deposition additive manufacturing, Mater. Des. 146 (2018) 249–259.
[14] C.B. Sweeney, B.A. Lackey, M.J. Pospisil, T.C. Achee, V.K. Hicks, A.G. Moran, B.R. Teipel, M.A. Saed, M.J. Green, Welding of 3D-printed carbon nanotube–polymer composites by locally induced microwave heating, Sci. Adv. 3 (2017), e1700262, .
[15] S. Bhandari, R.A. Lopez-Anido, D.J. Gardner, Enhancing the interlayer tensile strength of 3D printed short carbon fiber reinforced PETG and PLA composites via annealing, Addit. Manuf. 30 (2019) 100922.
[16] C. Basgul, T. Yu, D.W. MacDonald, R. Siskey, M. Marcolongo, S.M. Kurtz, Does annealing improve the interlayer adhesion and structural integrity of FFF 3D printed PEEK lumbar spinal cages? J. Mech. Behav. Biomed. Mater. 102 (2020) 103455.
[17] V. Kishore, C. Ajinjeru, A. Nycz, B. Post, J. Lindahl, V. Kunc, C. Duty, Infrared preheating to improve interlayer strength of big area additive manufacturing (BAAM) components, Addit. Manuf. 14 (2017) 7–12.
[18] M. Luo, X. Tian, W. Zhu, D. Li, Controllable interlayer shear strength and crystallinity of PEEK components by laser-assisted material extrusion, J. Mater. Res. 33 (2018) 1632–1641.
[19] M. Luo, X. Tian, J. Shang, W. Zhu, D. Li, Y. Qin, Impregnation and interlayer bonding behaviours of 3D-printed continuous carbon-fiber-reinforced poly-ether-ether-ketone composites, Compos. Part A Appl. Sci. Manuf. 121 (2019) 130–138.
[20] S. Shaffer, K. Yang, J. Vargas, M.A. Di Prima, W. Voit, On reducing anisotropy in 3D printed polymers via ionizing radiation, Polymer 55 (2014) 5969–5979.
[21] B. Hu, X. Duan, Z. Xing, Z. Xu, C. Du, H. Zhou, R. Chen, B. Shan, Improved design of fused deposition modeling equipment for 3D printing of high-performance PEEK parts, Mech. Mater. 137 (2019) 103139.
[22] N.P. Levenhagen, M.D. Dadmun, Interlayer diffusion of surface segregating additives to improve the isotropy of fused deposition modeling products, Polymer 152 (2018) 35–41.
[23] N.P. Levenhagen, M.D. Dadmun, Reactive processing in extrusion-based 3D printing to improve isotropy and mechanical properties, Macromolecules 52 (2019) 6495–6501.
[24] Q. Li, W. Zhao, Y. Li, W. Yang, G. Wang, Flexural properties and fracture behavior of CF/PEEK in orthogonal building orientation by FDM: microstructure and mechanism, Polymers 11 (2019) 656.
[25] A.A. Stepashkin, D.I. Chukov, F.S. Senatov, A.I. Salimon, A.M. Korsunsky, S.D. Kaloshkin, 3D-printed PEEK-carbon fiber (CF) composites: structure and thermal properties, Compos. Sci. Technol. 164 (2018) 319–326.
[26] S. Berretta, R. Davies, Y.T. Shyng, Y. Wang, O. Ghita, Fused deposition modelling of high temperature polymers: exploring CNT PEEK composites, Polym. Test. 63 (2017) 251–262.
[27] N.S. Hmeidat, J.W. Kemp, B.G. Compton, High-strength epoxy nanocomposites for 3D printing, Compos. Sci. Technol. 160 (2018) 9–20.
[28] M. Regis, A. Bellare, T. Pascolini, P. Bracco, Characterization of thermally annealed PEEK and CFR-PEEK composites: structure-properties relationships, Polym. Degrad. Stab. 136 (2017) 121–130.
[29] D.J. Blundell, B.N. Osborn, The morphology of poly(aryl-ether-ether-ketone), Polymer 24 (1983) 953–958.
[30] L. Zhou, J. Fu, Q. Gao, P. Zhao, Y. He, All-printed flexible and stretchable electronics with pressing or freezing activatable liquid-metal–silicone inks, Adv. Funct. Mater. 30 (2020) 1906683.
[31] M.K. Hausmann, P.A. Rühs, G. Siqueira, J. Läuger, R. Libanori, T. Zimmermann, A.R. Studart, Dynamics of cellulose nanocrystal alignment during 3D printing, ACS Nano 12 (2018) 6926–6937.
[32] R. Verker, E. Grossman, I. Gouzman, N. Eliaz, Trisilanolphenyl POSS–polyimide nanocomposites: structure–properties relationship, Compos. Sci. Technol. 69 (2009) 2178–2184.
[33] S. Yu, Y.H. Hwang, J.Y. Hwang, S.H. Hong, Analytical study on the 3D-printed structure and mechanical properties of basalt fiber-reinforced PLA composites using X-ray microscopy, Compos. Sci. Technol. 175 (2019) 18–27.
[34] H. Fan, R. Yang, Thermal decomposition of polyhedral oligomeric octaphenyl, octa (nitrophenyl), and octa(aminophenyl) silsesquioxanes, J. Therm. Anal. Calorim. 116 (2014) 349–357.
[35] A. Fina, D. Tabuani, F. Carniato, A. Frache, E. Boccaleri, G. Camino, Polyhedral oligomeric silsesquioxanes (POSS) thermal degradation, Thermochim. Acta 440 (2006) 36–42.
[36] M.M. Browne, M. Forsyth, A.A. Goodwin, The effect of solvent uptake on the relaxation behaviour, morphology and mechanical properties of a poly(ether ether ketone)/poly(etherimide) blend, Polymer 38 (1997) 1285–1290.

[37] T. Iqbal, B.J. Briscoe, P.F. Luckham, Surface plasticization of poly(ether ether ketone), Eur. Polym. J. 47 (2011) 2244–2258.
[38] M.C. Kuo, J.S. Kuo, M.H. Yang, J.C. Huang, On the crystallization behavior of the nano-silica filled PEEK composites, Mater. Chem. Phys. 123 (2010) 471–480.
[39] Y.H. Lai, M.C. Kuo, J.C. Huang, M. Chen, On the PEEK composites reinforced by surface-modified nano-silica, Mater. Sci. Eng. A 458 (2007) 158–169.
[40] A.R. Torrado, C.M. Shemelya, J.D. English, Y. Lin, R.B. Wicker, D.A. Roberson, Characterizing the effect of additives to ABS on the mechanical property anisotropy of specimens fabricated by material extrusion 3D printing, Addit. Manuf. 6 (2015) 16–29.
[41] S. Ahn, M. Montero, D. Odell, S. Roundy, P.K. Wright, Anisotropic material properties of fused deposition modeling ABS, Rapid Prototyp. J. 8 (2002) 248–257.
[42] S. Ziemian, M. Okwara, C.W. Ziemian, Tensile and fatigue behavior of layered acrylonitrile butadiene styrene, Rapid Prototyp. J. 21 (2015) 270–278.
[43] S. Rostom, M.D. Dadmun, Improving heat transfer in fused deposition modeling with graphene enhances inter filament bonding, Polym. Chem. 10 (2019) 5967–5978.
[44] O.S. Carneiro, A.F. Silva, R. Gomes, Fused deposition modeling with polypropylene, Mater. Des. 83 (2015) 768–776.
[45] A. Dorigato, V. Moretti, S. Dul, S.H. Unterberger, A. Pegoretti, Electrically conductive nanocomposites for fused deposition modelling, Synth. Met. 226 (2017) 7–14.
[46] L.J. Love, V. Kunc, O. Rios, C.E. Duty, A.M. Elliott, B.K. Post, R.J. Smith, C.A. Blue, The importance of carbon fiber to polymer additive manufacturing, J. Mater. Res. 29 (2014) 1893–1898.
[47] C.E. Duty, V. Kunc, B. Compton, B. Post, D. Erdman, R. Smith, R. Lind, P. Lloyd, L. Love, Structure and mechanical behavior of big area additive manufacturing (BAAM) materials, Rapid Prototyp. J. 23 (2017) 181–189.
[48] J.M. Chacón, M.A. Caminero, E. García-Plaza, P.J. Núñez, Additive manufacturing of PLA structures using fused deposition modelling: effect of process parameters on mechanical properties and their optimal selection, Mater. Des. 124 (2017) 143–157.
[49] R.T.L. Ferreira, I.C. Amatte, T.A. Dutra, D. Bürger, Experimental characterization and micrography of 3D printed PLA and PLA reinforced with short carbon fibers, Compos. Part B Eng. 124 (2017) 88–100.